A COMPUTATIONAL MODEL FOR THE FATIGUE STUDY: EFFECTS OF OVERLOAD, MEAN STRESS AND PLASTICITY ON PROPAGATION

Rafael Luis Moresco

Eduardo Bittencourt

Rafael_moresco01@yahoo.com.br

Eduardo.bittencourt@ufrgs.br

Universidade Federal do Rio Grande do Sul - UFRGS

99 Osvaldo Aranha Ave, 90035-190, Rio Grande do Sul, Porto Alegre, Brazil

Guilherme Fiorin Fornel

Gulherme.fornel@ufrgs.br

Universidade Federal do Rio Grande do Sul

99 Osvaldo Aranha Ave, 90035-190, Rio Grande do Sul, Porto Alegre, Brazil

Abstract. *The fatigue crack growth is analyzed numerically using a finite element platform, where the fracture problem is treated discretely by cohesive interface elements. The studied cases are restricted to plane strain and only subjected to the normal opening between the surfaces of the crack. The separation of crack interfaces is described by the use of two models of irreversible cohesive zone, one with displacement to the origin and another with residual opening. The models have traction-separation relationships that do not follow a predefined path, being dependent on the evolution of the damage linked to the properties of the cohesive zone. Initially, basic uniaxial responses for the cohesive elements are shown. Then, model is applied in the analysis of the fatigue crack growth in a double cantilever beam, where the observed structure is formed by the union of two metal plates through a cohesive adhesive that directs the growth of the crack. Cases with single amplitude overload are computed to demonstrate the effects on the propagation. In addition, a transient fatigue analysis is performed through responses generated by the application of block loading sequences. The implemented computational model qualitatively reproduces the results presented in reference works for the analyzed problems.*

Keywords: *Cracks growth, Cohesive zone model, Transient fatigue*

1 INTRODUCTION

The mechanisms that guide the growth of cracks in interfaces on quasi-static loads have already been explored, but fatigue crack growth (FCG) in interfaces still remains a doubt. In many studies, the factor that determines crack growth is described by the use of Paris (1961) equation. According to Bailon and Antolovich (1983), this method based on Eq. (1) provides a data correlation scheme, through a relation between the propagation rate da/dN and the stress intensity factor range ΔK, instead of predicting results.

$$\frac{da}{dN} = C(\Delta K)^m \tag{1}$$

The Paris method is applicable under small-scale propagation conditions, and during the calculation process the value of ΔK remains constant in all increments, which is not consistent with the actual conditions. Yao and Shang (1997), reported that the values of the constants C and m have a connection with the mixed mode of propagation, and this effect is attributed to changes in the mechanism of damage that acts at the interface and to variations in the strain-strain fields in the vicinity of the crack tip. For Roe and Siegmund (2003), the knowledge of these implications cannot be obtained using the results of monotonic loading, since the dependence of geometry and the question of the crack closure by fatigue introduces additional complexities. In addition, sometimes interface failure is linked to crack bridging events and, if a zone where this phenomenon occurs has a size comparable to some dimension of the problem, conditions for the use of Paris may be violated.

Other methodologies have been proposed to address the shortcomings of the Paris law. The concept of integral J of the nonlinear fracture was used to treat fatigue problems involving large scale. Dowling and Begley (1976) proposed their use for the calculation of the fracture energy ΔG, and then applied it in the Paris law. The problem is that this type of application is complex to be evaluated due to integration operations. Another methodology followed involves the use of models based on geometric correlations between the crack tip opening displacement (CTOD) and the crack advance. According to Roe and Siegmund (2003), a CTOD value cannot be assumed as a parameter of the material because it is dependent on mechanical limitations and the mixed loading mode. In addition, the process zone models also describe the FCG using the concept of accumulation of damage in a zone at the crack tip, which hardens over a constant cyclic deformation until a critical damage state is reached. The main problems of this approach are the application of the Manson-Coffin law and the Palmgren-Miner rule, in addition to considering a fixed process zone size for the material.

The cohesive zone model (CZM), whose concept can be linked to the original cohesive models of Dugdale (1960) and Barenblatt (1962), has been successfully applied. Without the crack nucleation criterion used in classical fracture mechanics, CZM removes non-real stress singularities at the crack tip and considers crack growth a progressive process of material degradation. An important feature of the CZM approach is that it can be easily implemented in computational methods such as the Finite Element Method. Commonly, CZM is used to deal with fracture problems and therefore extended to predict fatigue fracture. This method was used to analyze the growth of fatigue cracks in adhesives (Moroni and Pirondi, 2011), composites (Harper and Hallett, 2010), rolled metals (Yamaguchi et al., 2009), welds (Yang, 2006), among others.

In the present work, the CZM of Needleman (1992) associated to the damage model of Roe and Siegmund (2003) is implemented in an algorithm where it is tried to evaluate situations in which the crack propagation occurs exclusively under mode I (opening) and plane strain for materials with different behaviors. Initially, responses of mono-elements subjected to cyclic loads are observed in the representation of fundamental fatigue behaviors. Then, on a double cantilever beam (DCB), the effect of load/unload transient cycles on the formation of the cohesive zone and the propagation of cracks is studied.

2 METHODOLOGY

The CZM formulation of Needleman (1992) is based on the principle of virtual works, building a relationship between cohesive tension and material separation. This law describes the separation of the material over monotonic loading through a potential energy function ϕ that has an interatomic origin. This energy depends on the updated values of the normal separation Δ_n and tangential Δ_t of the crack surfaces, and its derivative in relation to the separations generates the normal cohesive tensions T_n and shear T_t.

Taking the simplified model for the mode I of rupture, Eq. (2) expresses the relation of T_n as a function of Δ_n and Eq. (3) shows the cohesive energy of normal surface $\phi_{n,0}$. In these relations, there are two material parameters, the maximum initial cohesive stress on monotonic loading $\sigma_{max,0}$ and the cohesive length δ_0, which corresponds to the accumulated separation required for the material to reach $\sigma_{max,0}$.

$$T_n = \sigma_{max,0} \exp(1) \exp\left(-\frac{\Delta_n}{\delta_0}\right)\left(\frac{\Delta_n}{\delta_0}\right) \tag{2}$$

$$\phi_{n,0} = \sigma_{max,0}\delta_0 \exp(1) \tag{3}$$

The use of this configuration for the fatigue cracking simulation brings infinite life to the forecast, which is not consistent with the real conditions. Therefore, to capture the effect of finite life on fatigue, an evolution of damage during the cyclical process must be considered. Taking this process as non-linear for inelastic deformation, CZM can be established as an analogy of the principles of plasticity that allow the softening of the characteristic stress. The laws of evolution of elastic-plastic damage include the following considerations: (i) Damage begins its accumulation once a deformation measure, accumulated or current, is greater than a critical value; (ii) The increase in damage is related to the deformation increment weighted by the updated load level; (iii) There is a fatigue limit at which a lower stress level can be applied cyclically without causing accumulation of damage and subsequent failure.

The damage model of Roe and Siegmund (2003) incorporates the previous considerations to describe the setback of cohesive property of the material. The updated cohesive stress σ_{max} is related to $\sigma_{max,0}$ by the use of Eq. (4), where D_c corresponds to the accumulated damage.

$$\sigma_{max} = (1 - D_c)\sigma_{max,0} \tag{4}$$

According to Wang and Siegmund (2006), in order to obtain the updated state of the damage, a description of its development in the rate format, $\dot{D}_c = \dot{D}_c(T_n, \Delta_n, D_c)$, modeled by Eq. (5).

$$\dot{D}_c = \frac{|\dot{\Delta}_n|}{\delta_\Sigma}\left[\frac{T_n}{\sigma_{max}} - \frac{\sigma_f}{\sigma_{max,0}}\right] H(\Delta_{n,acc} - \delta_0) \tag{5}$$

The relation is dependent on a Heaviside H function, which allows the calculation of $\dot{D}_c$ only when the value of the accumulated opening $\Delta_{n,acc}$ is greater than δ_0. The value of $\Delta_{n,acc}$ is found by Eq. (6). Since $\dot{D}_c$ depends on the magnitude of the opening rate $|\dot{\Delta}_n|$ its value can exist both in the load process and in the unload process, being obligatorily positive or null.

$$\Delta_{n,acc} = \int_t |\dot{\Delta}_n| dt \tag{6}$$

In Eq. (5) two parameters of the cohesive zone of the material, the fatigue strength limit of the cohesive zone σ_f and the accumulated cohesive length δ_Σ are observed. The property δ_Σ has the function of weighing the value of $|\dot{\Delta}_n|$. The magnitude of $\dot{D}_c$ is proportional to the normalized separation increment, $|\dot{\Delta}_n|/\delta_\Sigma$.

The load/unload process, when taken to the origin, follows the stiffness $T_{n,max}/\Delta_{n,max}$, where $\Delta_{n,max}$ corresponds to the maximum opening reached in the previous loading cycle and $T_{n,max}$ the respective stress. This condition is described by Eq. (7). On the other hand, in case the process has residual displacements, the relation follows Eq. (8).

$$T_n = \left(\frac{T_{n,max}}{\Delta_{n,max}}\right) \Delta_n \tag{7}$$

$$T_n = T_{n,max} + \frac{\sigma_{max} \exp(1)}{\delta_0} (\Delta_n - \Delta_{n,max}) \tag{8}$$

During the unload process, there is the possibility of contact between the surfaces of the crack evidencing compression. For the model without residual displacement cohesive tension of compression, $T_{n,comp}$ is found through a modification in Eq. (2) in which a penalty $A = 30$ is applied in its stiffness, Eq. (9). When the unload process occurs with deformation Eq. (10) is taken, where $\alpha = 10$ (Roe and Siegmund, 2003).

$$T_{n,comp} = A\sigma_{max} \exp(1) \exp\left(-\frac{\Delta_n}{\delta_0}\right)\left(\frac{\Delta_n}{\delta_0}\right) \tag{9}$$

$$T_{n,comp} = T_n(\Delta_n) + T_{n,max} - \frac{\sigma_{max} \exp(1)}{\delta_0} \Delta_{n,max} + \alpha\sigma_{max,0} \exp(1) \exp\left(-\frac{\Delta_n}{\delta_0}\right)\left(\frac{\Delta_n}{\delta_0}\right) \tag{10}$$

Once the critical damage is reached, the cohesive stresses are replaced by contact stresses $T_{n,contact}$, obtained by Eq. (11), present when the opening is negative.

$$T_{n,contact} = \alpha\sigma_{max,0} \exp(1) \exp\left(-\frac{\Delta_n}{\delta_0}\right)\left(\frac{\Delta_n}{\delta_0}\right) \tag{11}$$

The CZM is implemented on the Metafor (Ponthot, 1995) platform where four-node dummy cohesive interface elements are used to represent the crack surfaces between the sides of adjacent real finite elements, as in Fig. (1). The cohesive element can move in the normal and tangential directions, where initially the two pairs of nodes (1, 4) and (2, 3) have the same coordinates. With the increments of stress, the nodes can separate or overlap generating cohesive stresses that are calculated through four Gaussian points. The breaking of the cohesive element is considered when one of the points presents $D_c \geq 1$.

3 APPLICATIONS

3.1 Mono-element without residual displacement

This analysis is performed on a single cohesive element subject to traction/separation relations that do not present residual deformation. The element is positioned between two finite elements in plane strain, as shown in Fig. (1). The design allows to evaluate exclusively the behavior of the cohesive element, without influence of the others. The material has the cohesive properties $\sigma_{max,0} = 1GPa$, $\delta_0 = 0.005mm$, $\delta_\Sigma = 4\delta_0$ and $\sigma_f = 0.25\sigma_{max,0}$. Cyclic prescribed displacements Δ_n in the directions β of three different magnitudes, 0.8, 0.6 and $0.4\delta_0$, are applied over the nodes of the cohesive element with periods t_c of two seconds.

Figure (2.a-c) shows the cohesive tensions T_n as a function of the openings Δ_n reported by the element interfaces in the cyclic process, both normalized. It is observed that the maximum displacements reached in each test are exactly those applied. The evolution of the accumulated damage D_c, until reaching the unit value, for each case is shown in Fig. (2.d). For the prescribed value of $0.8\delta_0$, it was required 8.3 load/unload cycles to reach the rupture, while for the $0.6\delta_0$ it was necessary 12.9 cycles, and finally to $0.4\delta_0$, 29.6 cycles.

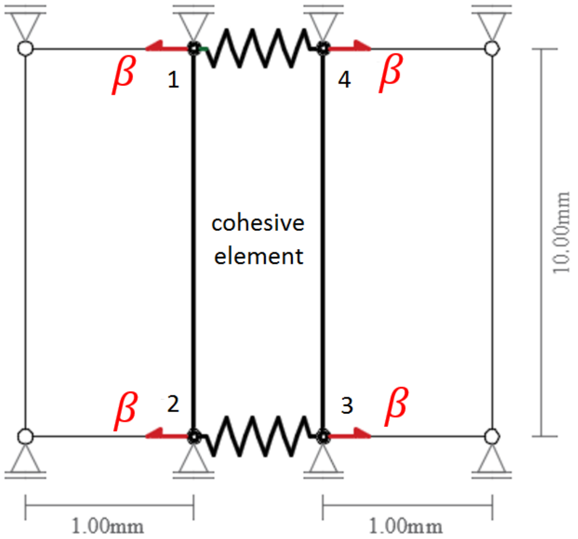

Figure 1. Schematic drawing depicting the model of applications 3.1 and 3.2

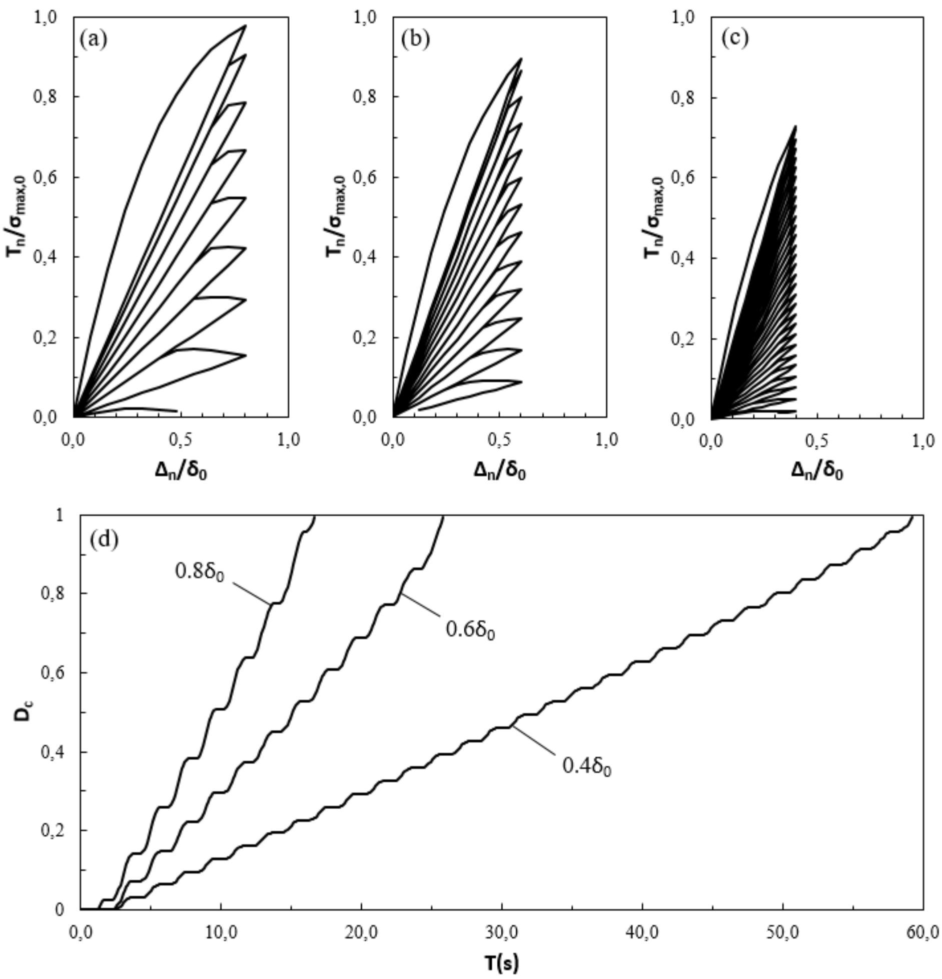

Figure 2. (a) Traction-separation behavior for 0,8δ$_0$; (b) 0,6δ$_0$; (c) 0,4δ$_0$. (d) Damage evolution behavior

3.2 Mono-element with residual displacement

The system of this application is analogous to that of the first case, Fig. (1), except that stresses in the β directions are applied and the load/unload law with residual displacement is used. The cohesive element incorporates properties characteristic of a high density polyethylene following the work of Siegmund (2004), which presents $\sigma_{max,0} = 6.66MPa$, $\delta_0 = 0.203mm$, $\delta_\Sigma = 4\delta_0$ and $\sigma_f = 0.25\sigma_{max,0}$.

Constant amplitude loading. The first step looks at finding the number of cycles for failure, N_f, of the cohesive element considering $D_c = 1$ and using a series of uniaxial loads that present different values of mean stress σ_{mean} and stress amplitude $\Delta\sigma$. The time t_c is two seconds. The values of N_f are shown in the mono-log plot of Fig. (3). Taking $\sigma_{mean} = 0$, a fatigue limit is established graphically, below which applied stresses do not cause damage to the material. This factor characterizes the infinite life conception in the fatigue analysis of the S-N curves. Increasing the value of σ_{mean} this limit tends to disappear. When comparing the N_f values of the present analysis with some of Siegmund (2004) work, a great similarity is observed where both reproduce responses typically found in fatigue studies.

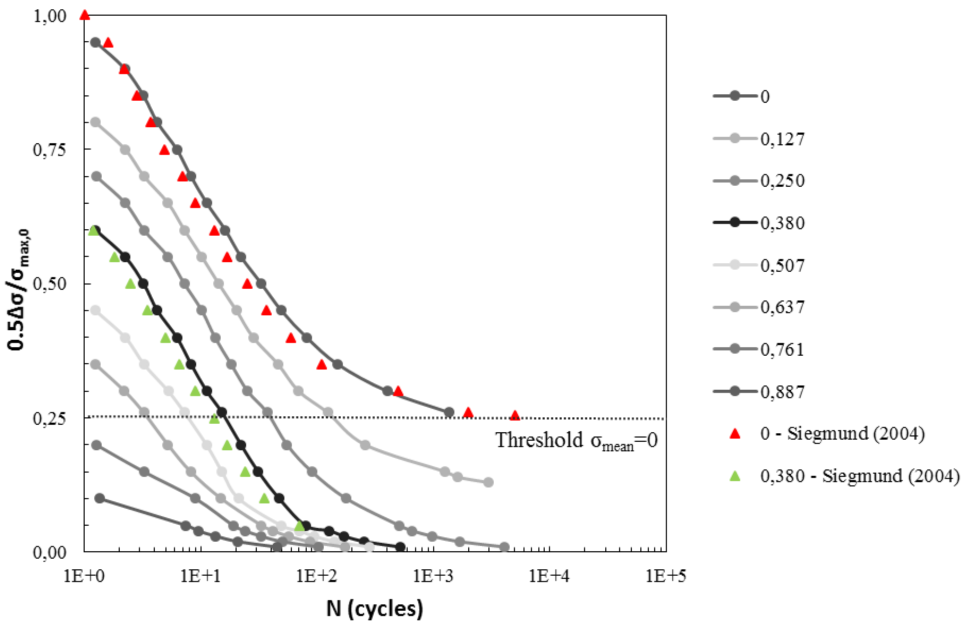

Figure 3. Number of cycles to failure for constant amplitude loading for several values of mean stress

Variable amplitude loading. The accumulation of damage is investigated when there is a variation of the stresses applied on the cohesive element. Two stresses values are applied in sequence, both with $\sigma_{mean} = 0$, where $(\Delta\sigma)_1$ is the first value and $(\Delta\sigma)_2$ is the second. Initially, the values of N_{f1} and N_{f2} are obtained, which correspond to the number of cycles for the element to fail, being applied only $(\Delta\sigma)_1$ and $(\Delta\sigma)_2$, respectively. Six cases were analyzed, Tab. (1). The answers obtained for each of the proposed situations are presented in Fig. (4), together with the values of the reference work and the Palmgren-Miner line. For Siegmund (2004), this is the most basic approach to describe fatigue through uniaxial efforts on varied amplitude. In Fig. (4), the abscissa axis represents the number of loading cycles $(\Delta\sigma)_1$ applied to the adhesive, where 1.0 indicates the single charge action. The axis of the ordinates denotes the same with respect to $(\Delta\sigma)_2$. The points in the graph represent the combinations of the cycle factors required to break the adhesive.

Table 1. Values of applied loads and corresponding failure cycles

	Case 01	02	03	04	05	06
$(\Delta\sigma)_1/2\sigma_{max,0}$	0.26	0.31	0.26	0.35	0.26	0.50
N_{f1}	1370	314	1370	150	1370.2	34
$(\Delta\sigma)_2/2\sigma_{max,0}$	0.31	0.26	0.35	0.26	0.50	0.26
N_{f2}	314	1370	150	1370	34	1370

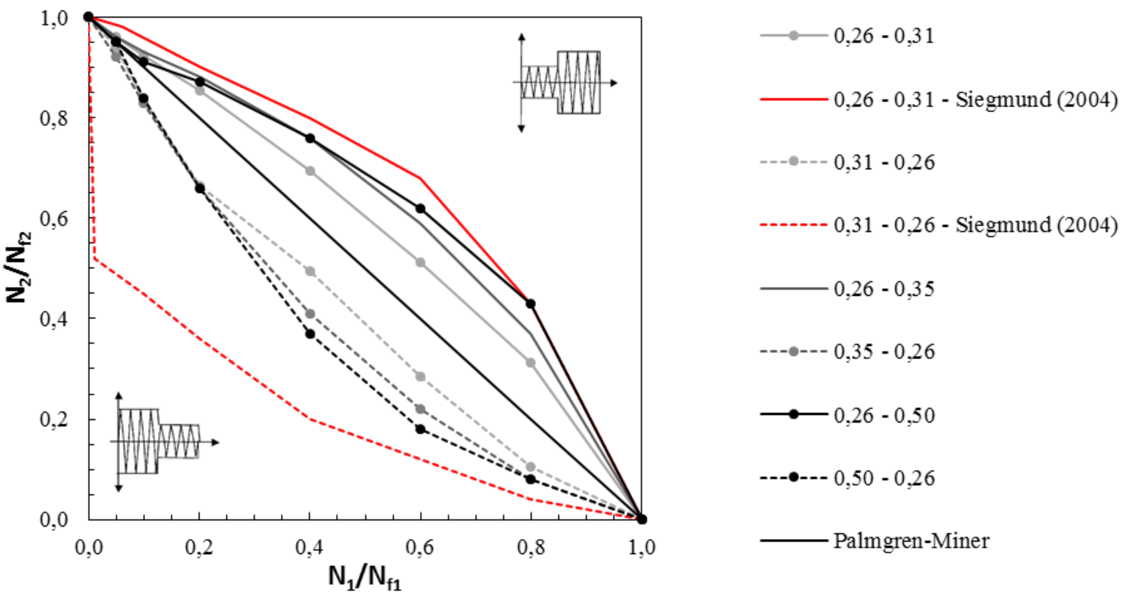

Figure 4. Number of cycles to failure during two different sequences of variable amplitude loading comparison to Palmgren-Miner rule

The accumulation of damage was shown to be non-linear, presenting greater variations in loading combinations between 20 and 80%. In the tests that have initial load of greater amplitude, the deviations of the line are absent when applied low numbers of cycles of the load $(\Delta\sigma)_1$. For Siegmund (2004), these differences were evidenced by the effect of the period necessary for the beginning of the accumulation of damage (related to variable $\Delta_{n,acc}$) on the number of cycles required for the rupture. In other words, smaller loads have a higher percentage of cycles N_f designed to "activate" the accumulation of damage, whereas for larger ones the opposite occurs, which would justify greater deviations from the linear relationship.

3.3 Transient loading in DCB

In this section, the analysis of crack growth on the action of transient fatigue in a DCB is carried out following Siegmund (2004). The structure represented by Fig. (5), is formed by the union of two metal sheets through a structural adhesive. Its main dimensions are length $L = 216mm$, total height $2h = 18.72mm$ and thickness $B = 25.4mm$. The structural adhesive has thickness $e = 0.2mm$ and a crack of initial size $a_0 = 127mm$. The same properties of the adhesive of application 3.2 are used, except when mentioned otherwise. The metal sheets have longitudinal modulus of elasticity $E = 70000GPa$ and poisson coefficient $\nu = 0.34$. The cyclic loading is applied incrementally in the beam through the point load ΔP, which is determined according to the fracture energy G for the structure. For the model employed, G can be found through Eq. (12) (Anderson, 2005). Thus, ΔP is represented by an energy release rate range ΔG, where $\Delta G = G_{max} - G_{min}$.

$$G = \frac{12P^2a_0^2}{B^2h^3E} \tag{12}$$

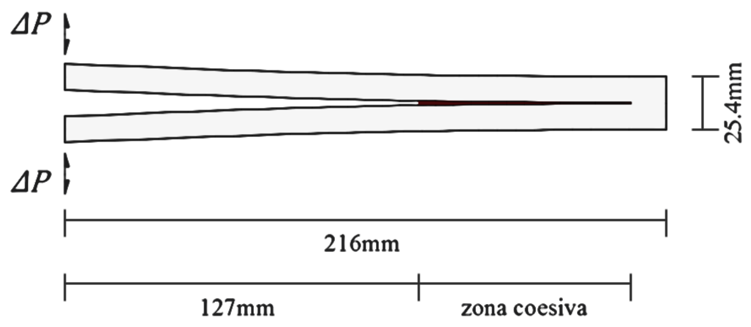

Figure 5. Schematic drawing depicting the DCB of application 3.3

The problem is modeled on finite elements considering that the crack propagates exclusively through the interface. The symmetry is used through constraints on vertical displacements in the horizontal symmetry axis. The node in which ΔP is applied has constraint in the horizontal direction. A total of 2843 quadrilateral plane strain elements and 190 cohesive interface elements (with length of $0.4mm$) that incorporate the residual displacement damage law are used. The values of the crack tip growth Δa_{tip}, the tip of the cohesive zone activated Δa_{cz} and the length of the cohesive zone l_{CZ}, are analyzed, where $l_{CZ} = \Delta a_{tip} - \Delta a_{cz}$ is considered. On the cohesive elements it is assumed that: (i) from the moment any of the Gaussian points of an element has $D_c > 0$ this is incorporated in l_{CZ}; (ii) when some point reaches $D_c = 1$ we have the element breaking and subsequent propagation of Δa_{cz}.

Constant amplitude loading. The structure is subjected to constant amplitude loadings and factor R equal to zero, whereas $R = G_{min}/G_{max}$. Values of ΔP are obtained from Eq. (12), where ΔG assumes percentages of $\phi_{n,0}$. In Fig. (6.a) the growth of Δa_{cz}, normalized by δ_0, as a function of N is shown for some relations of $\Delta G/\phi_{n,0}$ used. It is observed that the lower the applied load the higher the N value necessary for a given propagation to occur. The crack propagation velocity can be obtained from the initial derivative with respect to the time of each of the curves generated. This value is associated with $\Delta G/\phi_{n,0}$ following the Paris relation in the format of Eq. (13).

$$\frac{d(\Delta a_{cz}/\delta_0)}{dN} = m\left(\frac{\Delta G}{\phi_{n,0}}\right)^a \tag{13}$$

Figure (6.b) shows the data reported for this relationship, highlighting the threshold of fatigue and the point where static failure occurs. Approximating the relation by a power curve, the constants $m = 206.61$ e $a = 1.7575$ are found. The lower limit in which the fatigue propagation does not occur corresponds to the load ΔP which leads to values of Δ_n, and respective T_n, magnitudes insufficient for the occurrence of damage accumulation and subsequent propagation of Δa_{cz}, being associated here to the ratio $\Delta G/\phi_{n,0} = 0.004$. Siegmund (2004) reported different data leading to other constants. The author points out a range of applicability of the Paris ratio, which occurs between the energy ratio $\Delta G/\phi_{n,0} = 0.05$ and the static failure, and for energy ratios located between the fatigue threshold and the value of 0.05, the behavior does not follow Paris.

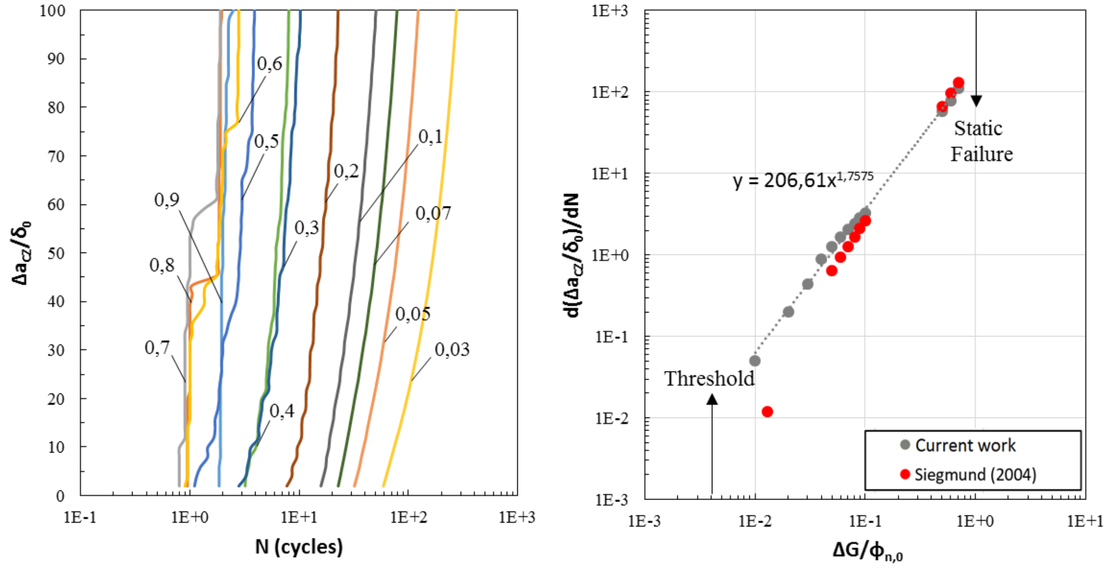

Figure 6. (a) Fatigue crack extension in dependence of the number of the applied load cycles for different applied energy release rate ranges; (b) Predicted dependence of normalized FCG rate on the normalized applied energy release rate range

Block loading: overload. The beam is subjected to a basic cyclic load with the value of $\Delta G/\phi_{n,0} = 0.0303$ for 120 cycles, followed by a 20-cycle overload block with value of $\Delta G/\phi_{n,0} = 0.0776$, both with $R = 0$. After the overload is applied, the basic cycle is resumed.

Figure (7) depicts the development of $\Delta a_{tip}/\delta_0$ and $\Delta a_{cz}/\delta_0$ compared to the values of Siegmund (2004). The first loading cycles denote the formation of the cohesive zone l_{CZ} with rapid growth, where $\Delta a_{tip}/\delta_0$ reaches a value of 50 after 7 cycles. From cycle 8, $\Delta a_{tip}/\delta_0$ develops almost constantly, with some abrupt variation in cycle 76, until the moment the overload is applied. The crack initiates its growth in cycle 58, where $\Delta a_{cz}/\delta_0$ follows a behavior very close to linear until the beginning of the overload. Shortly before the block is applied, l_{CZ}/δ_0 reaches the value of 59. At the moment the structure is subjected to overload, $\Delta a_{tip}/\delta_0$ shows a sudden increase of 14, and then follows with a more pronounced growth. Likewise, $\Delta a_{cz}/\delta_0$ has an increase in its growth velocity but not in a pronounced manner as $\Delta a_{tip}/\delta_0$. Thus, l_{CZ}/δ_0 has an amplitude of 73. After the passage through the 20-cycle block, the growth of $\Delta a_{tip}/\delta_0$ is practically interrupted for 43 cycles and then resumes at a rate very close to that which it possessed before applying the overload. $\Delta a_{cz}/\delta_0$ faces a deceleration and returns to values similar to those presented previously. Hence, l_{CZ}/δ_0 shrinks to the initial size of 59.

The evolution of $T_n/\sigma_{max,0}$ as a function of Δ_n/δ_0, for the point $x = a_0 + 45{,}3\delta_0$ is shown in Fig. (8.a). This point is part of l_{CZ} at the time the overload is applied. The overload generates large amplitudes at the interface openings and consequently high stresses, which lead to greater accumulations of damage, as observed in Fig. (8.b) where the development of D_c with respect to N for the same point is shown.

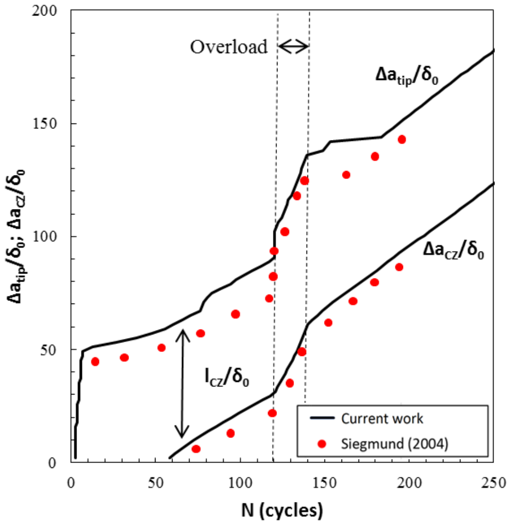

Figure 7. Location of the crack tip and the cohesive tip in dependence of the number of applied cycles for an overload block

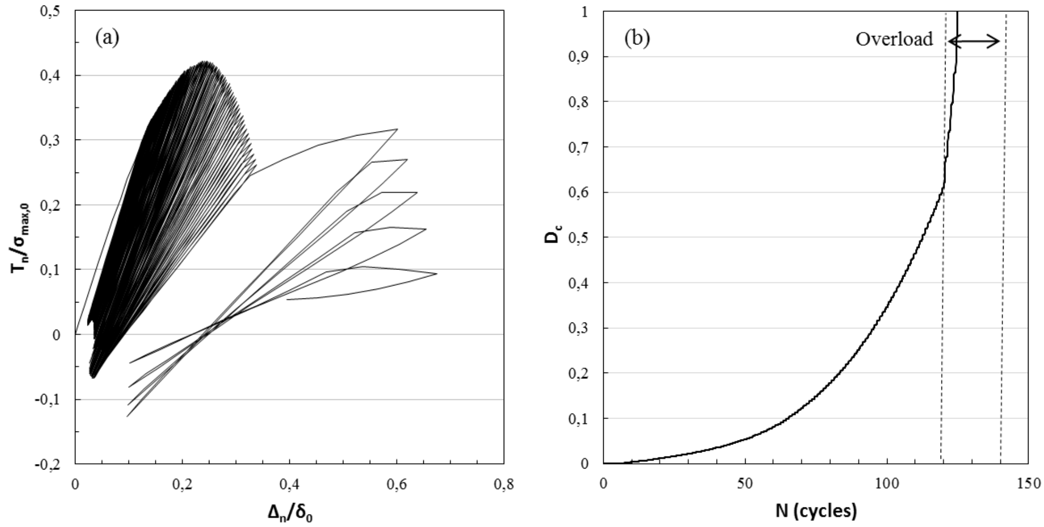

Figure 8. (a) Transient traction-separation behavior; (b) Predict damage evolution

Block loading: variable amplitude. The beam is subjected to a basic cyclic loading with the value of $\Delta G/\phi_{n,0} = 0.0776$ for 30 cycles with $R = 0$, followed by a block of 30 cycles with $G_{max}/\phi_{n,0} = 0.0776$ and $R = 0.75$. After the variable amplitude loading is applied, the basic cycle is resumed.

Figure (9) depicts the development of $\Delta a_{tip}/\delta_0$ and $\Delta a_{cz}/\delta_0$ compared to the results of Siegmund (2004). During the initial cycles of loading there is a rapid growth of l_{CZ}/δ_0, where $\Delta a_{tip}/\delta_0$ reaches the value 60 after 7 cycles. From cycle 8, $\Delta a_{tip}/\delta_0$ shows a linear development with a slight change between cycles 20 and 25. The crack begins its growth in cycle 20, where $\Delta a_{cz}/\delta_0$ presents a linear behavior until the beginning of the load with variable amplitude. Shortly before the block is applied l_{CZ}/δ_0 equals 77. At the instant the structure is subjected to variable amplitude, Δa_{tip} presents a slight delay in the growth

Proceedings of the XXXVIII Iberian Latin-American Congress on Computational Methods in Engineering
P.O. Faria, R.H. Lopez, L.F.F. Miguel, W.J.S. Gomes, M. Noronha (Editores), ABMEC, Florianópolis, SC, Brazil, November 5-8, 2017.

velocity and follows this way until the end of the block. Similarly, Δa_{cz} also shows decrease. During block l_{CZ}/δ_0 remains equal to 77. After the passage of 30 cycles, both Δa_{tip} and Δa_{cz} resume the propagation speeds shown previously. Between cycles 76 and 79, $\Delta a_{tip}/\delta_0$ shows a jump equal to 14.

Figure (10.a) shows the evolution of $T_n/\sigma_{max,0}$ as a function of Δ_n/δ_0 for the point $x = a_0 + 37{,}44\delta_0$. At the instant that the point is subjected to load with varied amplitude both Δ_n and T_n present smaller variations which determines a smaller accumulation of damage retarding the rupture, as reported in Fig. (10.b).

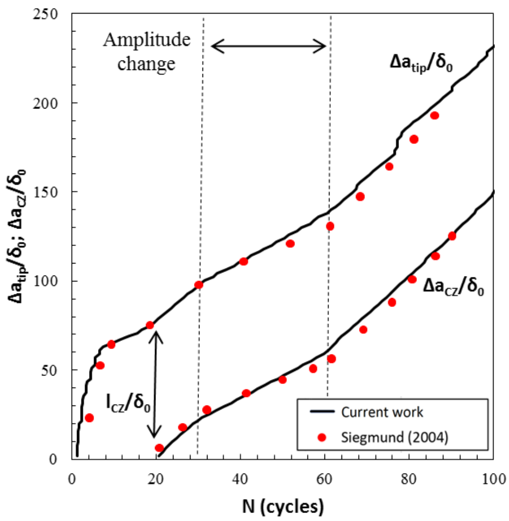

Figure 9. Location of the crack tip and the cohesive tip in dependence of the number of applied cycles for a variable amplitude block

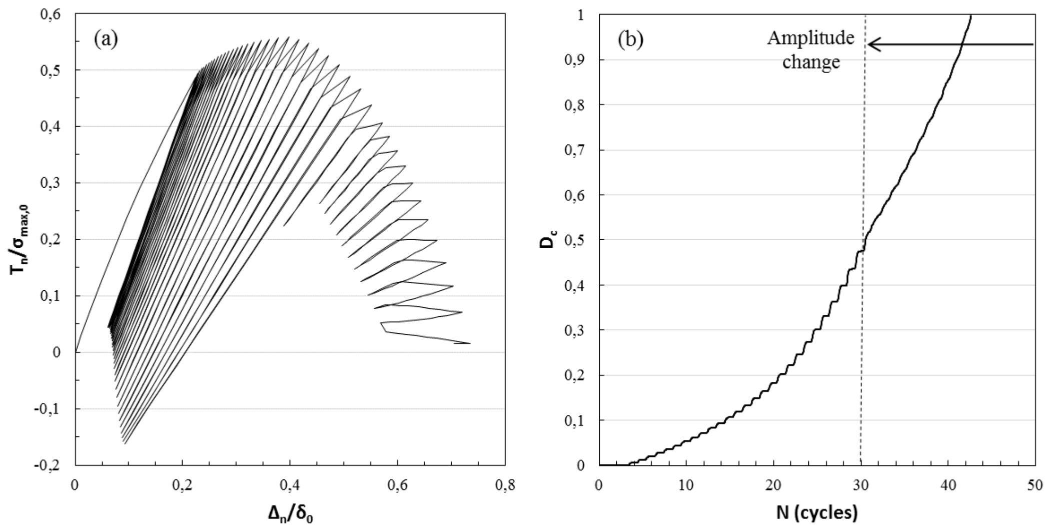

Figure 10. (a) Transient traction-separation behavior; (b) Predict damage evolution

Single overloads. The effects of the variations on the parameters that define the cohesive zone are evaluated, using a basic load of $\Delta G/\phi_{n,0} = 0.078$ with $R = 0$. The overload of $\Delta G/\phi_{n,0} = 0.175$ and $R = 0$ has a one-cycle performance, being applied at the moment that

Δa_{cz} reaches the length of $25\delta_0$. For comparative purposes tests are performed without overload.

In the first step, we observe the variation of the accumulated cohesive length. Three values are taken for the variable, $\delta_\Sigma = 3\delta_0$, $4\delta_0$ and $5\delta_0$. The fatigue limit is set at $\sigma_f = 0.25\sigma_{max,0}$. The results found for the growth of Δa_{cz} e Δa_{tip} are shown in Fig. (11.a-c), where dotted lines symbolize loading in the absence of overload. A clear increase in Δa_{tip} is observed in all tests at the time the overload is applied. The $\Delta a_{tip}/\delta_0$ jumps show similar values for the three models, around 29. On the other hand, Δa_{cz} shows only a slight increase in relation to the absent model of overload. For the case that considers $\delta_\Sigma = 3\delta_0$, the activated cohesive zone l_{CZ}/δ_0 counts 73 before the overload and 75 after the overload (with Δa_{tip} already in stabilized growth). For the case of $\delta_\Sigma = 4\delta_0$, these values rise to 75 and 76, and when $\delta_\Sigma = 5\delta_0$, 76 and 79.

According to Eq. (5), regarding the increase in damage, it is expected that a change in the value of δ_Σ directly reflects the amount of damage recorded. An increase in the value of δ_Σ generates a smaller damage value, when compared to the standard value of $4\delta_0$, and consequently a growth of Δa_{tip} and Δa_{cz} slower. Likewise, a decrease in δ_Σ leads to an increase in the development of the same variables. This forecast can be exemplified by the number of cycles required for $\Delta a_{tip}/\delta_0$ to reach 150. 40 cycles are required when $\delta_\Sigma = 3\delta_0$, 53 cycles when $\delta_\Sigma = 4\delta_0$ and 69 cycles for $\delta_\Sigma = 5\delta_0$.

In the second step, three values are estimated for the fatigue limit, $\sigma_f = 0.15\sigma_{max,0}$, $0.25\sigma_{max,0}$ and $0.4\sigma_{max,0}$, with the accumulated cohesive length set at $\delta_\Sigma = 4\delta_0$. The values found for the development of Δa_{tip} and Δa_{cz} are shown in Fig. (11.b, d, e). Again, all three cases point to a jump in the values of Δa_{tip} when overloading is applied. At this point Δa_{cz} also experiences variations with different magnitudes, being larger in the model of $0.15\sigma_{max,0}$ and almost null in the model of $0.4\sigma_{max,0}$. The size of l_{CZ} presents changes according to the ratio of the applied fatigue limit. In the case of $\sigma_f = 0.15\sigma_{max,0}$ the value of l_{CZ}/δ_0 before the overload is 87 and after 81. For the structure subject to $0.25\sigma_{max,0}$ these values fall to 75 and 76. And, for $0.4\sigma_{max,0}$ the smaller sizes of l_{CZ}/δ_0, 71 and 65, before and after the overload respectively.

Through Eq. (5) it can be concluded that the activation of the cohesive zone, reflected by the growth of Δa_{tip}, has dependence related to the fatigue limit. Low values of σ_f allow early activation, while high values delay the same. In the same way, Δa_{cz} can present a brief growth if σ_f is a small value, which allows a greater accumulation of damage per cycle or, to have a deceleration in the growth if σ_f is of great magnitude. The time required for $\Delta a_{cz}/\delta_0$ to reach 80 can be cited as an example. Considering $\sigma_f = 0.15\sigma_{max,0}$ 30 cycles are used, while for $0.25\sigma_{max,0}$ 57 cycles are required, and finally 86 cycles for the model employing $0.4\sigma_{max,0}$.

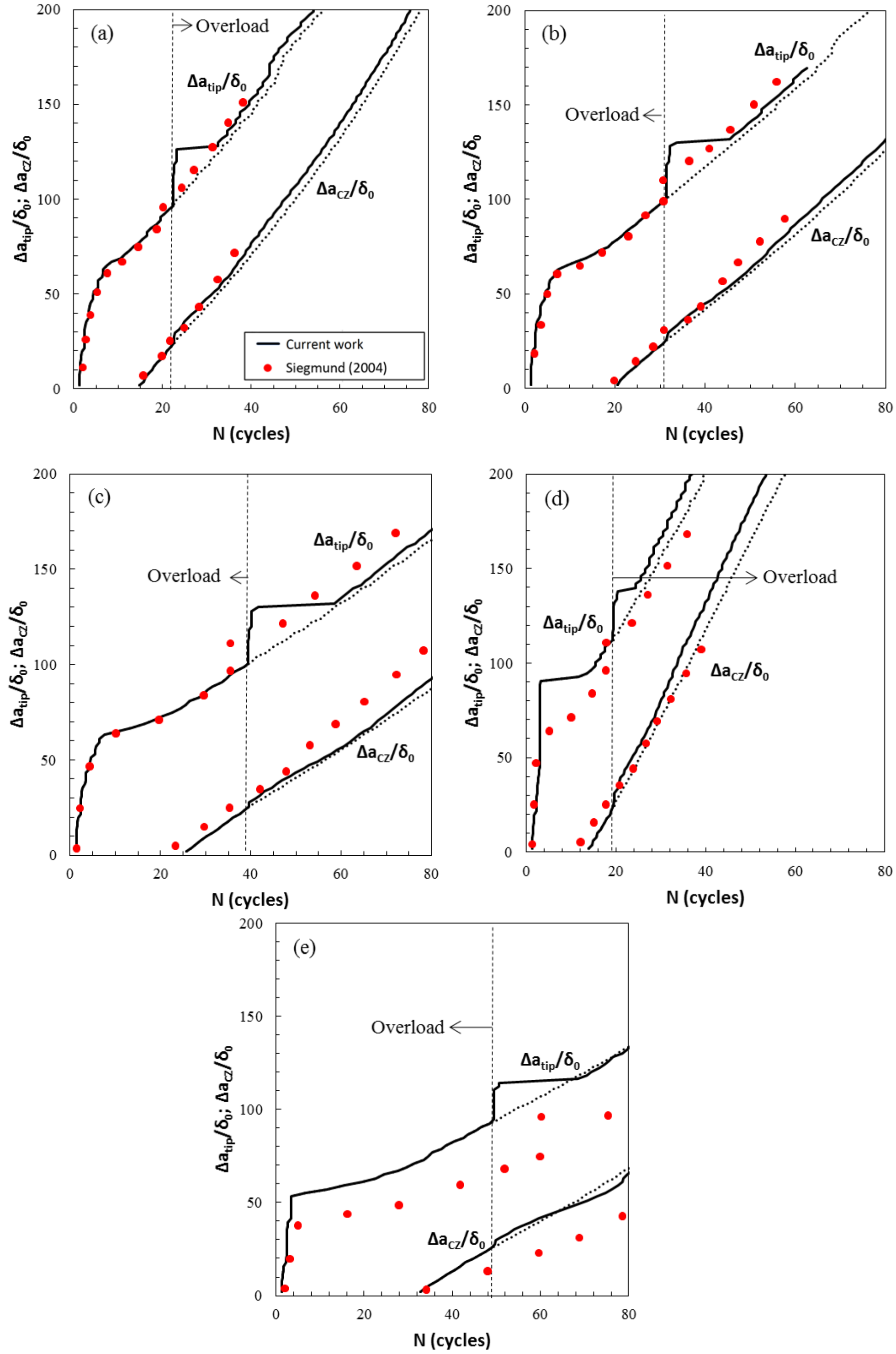

Figure 11. (a) Location of the crack tip and the cohesive tip in dependence of the number of applied cycles for a single overload $\sigma_f = 0.25\sigma_{max,0}$, $\delta_\Sigma = 3\delta_0$; (b) $\sigma_f = 0.25\sigma_{max,0}$, $\delta_\Sigma = 4\delta_0$; (c) $\sigma_f = 0.25\sigma_{max,0}$, $\delta_\Sigma = 5\delta_0$; (d) $\sigma_f = 0.4\sigma_{max,0}$, $\delta_\Sigma = 4\delta_0$; (e) $\sigma_f = 0.15\sigma_{max,0}$, $\delta_\Sigma = 4\delta_0$;

4 CONCLUSION

The applications involving mono-elements simulated with quality the expected behavior on constant loads, representing patterns such as the S-N curves and the fatigue limit stress. With respect to the loads of varied amplitudes applied in sequence, the results pointed out deviations of the linear relation of magnitudes different from those found in the reference work. Considering the application in the DCB beam, its results can be framed in a Paris law, with lower loads showing greater deviations from the reference work. As reported in Siegmund (2004), loadings in which changes occur in the values of ΔG, under constant value of R, lead to transient accelerations and decelerations in the crack growth rates, being these changes connected to the cohesive zone, denoting a direct relation Between its size and the speed of propagation. On the other hand, loads that vary only R have changes in the crack growth rate, without demonstrating transition zones and under constant cohesive zone size. Also, the application of single overloads on the structure did not provoke growth of the propagation velocity, with only Δa_{tip} developing in a marked way after the passage, followed by a number of cycles which did not evolve, resuming the growth soon after.

The differences found between the works can have diverse origins. The finite element size and its distribution density; The number of Gaussian points and the interpolation functions of the cohesive elements; And finally, the linear application of the loads in the structure, in contrast with Siegmund's (2004) sinusoidal shape, can be considered as the cause of the disagreements.

Acknowledgements

To Coordenação de Aperfeiçoamento de Pessoal de Nível Superior (Capes) for the support of the research.

REFERENCES

Anderson, T. L., 2005. *Fracture mechanics: fundamentals and applications*. CRC press.

Bailon, J. P., & Antolovich, S. D., 1983. Effect of microstructure on fatigue crack propagation: a review of existing models and suggestions for further research. In *Fatigue Mechanisms: Advances in Quantitative Measurement of Physical Damage*. ASTM International.

Barenblatt, G. I., 1962. The mathematical theory of equilibrium cracks in brittle fracture. *Advances in applied mechanics*, vol. 7, pp. 55-129.

Dowling, N. E., & Begley, J. A., 1976. Fatigue crack growth during gross plasticity and the J-integral. In *Mechanics of crack growth*. ASTM International.

Dugdale, D. S., 1960. Yielding of steel sheets containing slits. *Journal of the Mechanics and Physics of Solids*, vol. 8, n. 2, pp. 100-104.

Harper, P. W., & Hallett, S. R., 2010. A fatigue degradation law for cohesive interface elements–development and application to composite materials. *International Journal of Fatigue*, vol. 32, n. 11, pp. 1774-1787.

Moroni, F., & Pirondi, A., 2011. A procedure for the simulation of fatigue crack growth in adhesively bonded joints based on the cohesive zone model and different mixed-mode propagation criteria. *Engineering Fracture Mechanics,* vol. 78, n. 8, pp. 1808-1816.

Needleman, A., 1992. Micromechanical modelling of interfacial decohesion. *Ultramicroscopy*, vol. 40, n. 3, pp. 203-214.

Paris, P. C., Gomez, M. P., & Anderson, W. E., 1961. A rational analytic theory of fatigue. *The trend in engineering*, vol. 13, n. 1, pp. 9-14.

Ponthot, J. P., 1995. *Traitement unifié de la Mécanique des Milieux Continus solides en grandes transformations par la méthode des éléments finis*. Doctoral thesis, Université de Liège.

Roe, K. L., & Siegmund, T., 2003. An irreversible cohesive zone model for interface fatigue crack growth simulation. *Engineering fracture mechanics*, vol. 70, n. 2, pp. 209-232.

Siegmund, T., 2004. A numerical study of transient fatigue crack growth by use of an irreversible cohesive zone model. *International Journal of Fatigue*, vol. 26, n. 9, pp. 929-939.

Yamaguchi, T., Okabe, T., & Yashiro, S., 2009. Fatigue simulation for titanium/CFRP hybrid laminates using cohesive elements. *Composites Science and Technology,* vol. 69, n. 11, pp. 1968-1973.

Yang, S. Y., 2006. Analysis of fatigue crack growth in weld specimen using three-dimensional cohesive zone model. In *Key Engineering Materials,* vol. 321, pp. 674-677. Trans Tech Publications.

Yao, D., & Shang, J. K., 1997. Effect of load-mix on fatigue crack growth in 63Sn-37Pb solder joints. *Transactions-American Society Of Mechanical Engineers Journal Of Electronic Packaging*, vol. 119, pp. 114-118.

Wang, B., & Siegmund, T., 2006. A computational analysis of size effects in fatigue failure. *Modelling and Simulation in Materials Science and Engineering*, vol. 14, n. 4, pp. 775.